Hindawi Publishing Corporation
International Journal of Antennas and Propagation
Volume 2016, Article ID 7439403, 9 pages
http://dx.doi.org/10.1155/2016/7439403

Research Article

On-Body Characterization of Planar Differential Antennas for Multiple, Wide, and Narrow Bands

Luigi Vallozzi,[1] Domenico Pepe,[2,3] Thijs Castel,[1] Hendrik Rogier,[1] and Domenico Zito[2,4]

[1]*Department of Information Technology, Ghent University-iMinds, Technologiepark Zwijnaarde 15, 9052 Gent, Belgium*
[2]*Tyndall National Institute, Lee Maltings, Dyke Parade, Cork T12 R5CP, Ireland*
[3]*DISMI, University of Modena and Reggio Emilia, Via Amendola 2, 42122 Reggio Emilia, Italy*
[4]*School of Engineering, University College Cork, College Road, Cork T12 RXA9, Ireland*

Correspondence should be addressed to Domenico Zito; domenico.zito@tyndall.ie

Received 2 February 2016; Revised 2 June 2016; Accepted 26 June 2016

Academic Editor: Antonio Faraone

This paper reports the results of the on-body experimental tests of a set of four planar differential antennas, originated by design variations of radiating elements with the same shape and characterized by the potential for covering wide and narrow bands. All the antenna designs have been implemented on low-cost FR4 substrate and characterized experimentally through on-body measurements. The results show the impact of the proximity to the human body on antenna performance and the opportunities in terms of potential coverage of wide and narrow bands for future ad hoc designs and implementations through wearable substrates targeting on-body and off-body communication and sensing applications.

1. Introduction

UWB radar for contactless detection of respiratory rate of human beings [1–4] is an active research area requiring innovative transceiver and antenna developments [5, 6]. A novel planar differential antenna was proposed recently by our research group [7]. This antenna was designed to meet the design constrains, electromagnetic performance, and physical integration, required by the ultrawideband (UWB) pulse radar sensor operating approximately in the frequency band from 3 to 5 GHz [2–4]. The proximity between the radiating elements of the proposed differential antenna has allowed achieving a significant bandwidth enhancement. In addition to original differential antenna development, we also investigated some design variations with the objective of showing how these reflect on the antenna performance, showing that the antennas originating from radiating elements with the same shape can be potentially adopted through an agile design strategy to cover wide and narrow bands of interest for a number of wireless applications, communication, and sensing, as a consequence of variations in size and orientation of the radiating elements with respect to the original planar differential antenna [8].

Numerous studies were carried out about the effects of human body on performance of planar antennas. Concerning *nondifferential* antennas, many contributions reported the effects on S-parameters and gain patterns, like in [9, 10]. Considering *differentially fed* antennas, in [11], the in-body near-field radiation pattern of an on-body antenna was characterized. In other studies, implantable antennas were considered, like in [12, 13], where the in-body radiation patterns and S-parameters were investigated. However, to the authors' knowledge, the experimental characterization of differential antennas on human body, in terms of *off-body far-field* radiation patterns, which is proposed in the present paper, has received no attention yet in existing literature.

Fully differential transceivers are less prone to common-mode noise and interferers; thereby differential antennas could play a significant role in future networks and communications, especially considering the massive amount of devices envisaged for the Internet of Things era [14, 15] that

are supposed to operate in regions of frequency spectrum already crowded by existing applications and services.

In this paper, we report for the first time the results of the on-body experimental characterization of the variations of planar differential antenna design described in [8], resulting from measurements on a real human subject, which have not been reported in any of our previous publications. For reasons of space, the details and results of previous publication [8] will be not repeated here. Thereby, for the insights about the design, inherent properties, and free-space (in air) performances of the antennas, we invite the reader to inspect our previous work reported in [8]. In particular, in this work, here, we will show for the first time how the proximity to the human body affects the antenna performance and that the antennas, all originating from radiating elements with the same shape, can be potentially adopted in future ad hoc designs on flexible substrates or textile fabrics to cover multiple, wide, and narrow bands of interest for a number of wearable applications for both communication and sensing [16].

The paper is organized as follows. Section 2 reports the description of the antenna design variations and summarizes, for reasons of self-consistency, the main results obtained from the previous free-space tests, which provide the term of reference for design and performance. Section 3 reports the measurement results obtained from the tests on a real human body. Finally, in Section 4, the conclusions are drawn.

2. Planar Differential Antennas: Designs and Tests

Two different sets of planar differential antennas were designed on a low-cost FR4 substrate ($\varepsilon_r = 4.4$, dielectric thickness $T = 1.6$ mm, copper thickness $t = 35\,\mu$m, and loss tangent $\tan\delta = 0.02$) for a complete characterization as stand-alone devices. The layout drawing of the first set of antennas, namely, *folded planar differential antennas*, is shown in Figure 1. The layout drawing of the second set of antennas, being *antipodal planar differential antennas*, is shown in Figure 2. At first glance, we observe that each radiating element of the antenna consists of a semicircle and a triangle that provides a smooth transition towards the input pins [7]. In particular, in the folded planar differential antenna, the two radiating elements are folded one aside the other. In particular, the design is characterized by the aperture angle of triangle α and rotation angle ρ between the symmetry axes of the two radiating elements. The main features of this design approach are that it allows a compact design of both the transmitter and receiver antennas on the same board of the implemented radar sensor based on a system-on-a-chip radar transceiver, still maintaining good performance [2–4]. In the antipodal planar differential antenna, the two radiating elements are rotated by 180° one with respect to the others, so resulting in an antipodal position.

In the following subsections, we will summarize the results obtained for the experimental open-space tests. In

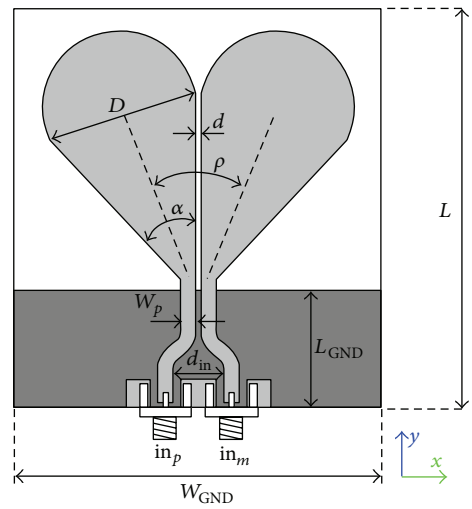

Figure 1: Layout drawing of the folded planar differential antennas. The top copper layer is in light grey and the bottom copper layer is in dark grey.

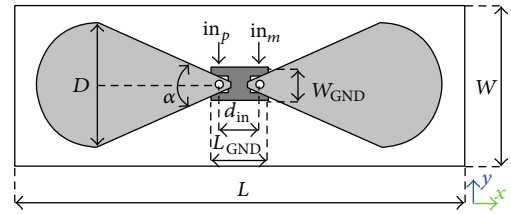

Figure 2: Layout drawing of the antipodal planar differential antennas. The top copper layer is in light grey and the bottom copper layer is in dark grey.

particular, we report the results of two antenna designs for each set, folded and antipodal, as follows:

(A) Folded planar differential antenna with $\rho = 45°$ and $D = 3$ cm, as shown in Figure 1.

(B) Folded planar differential antenna with $\rho = 45°$ and $D = 4$ cm, as shown in Figure 1.

(C) Antipodal planar differential antennas with $\rho = 180°$ and $D = 3$ cm, as shown in Figure 2.

(D) Antipodal planar differential antennas with $\rho = 180°$ and $D = 4$ cm, as shown in Figure 2.

All the antenna designs were carried out by means of the electromagnetic (EM) simulator Momentum by Keysight Technologies®, and characterized experimentally in anechoic chamber.

2.1. Folded Radiating Elements: $\rho = 45°$ and $D = 3$ cm. The physical implementation is shown in Figure 3. Distance d between the two sides of the antenna is equal to 1 mm. Diameter D is equal to 3 cm in order to resonate at the frequency of interest (i.e., roughly 3 GHz). The aperture angle of the triangle is $\alpha = 45°$. The rotation angle of the two radiating elements is $\rho = 45°$.

Table 1: Folded planar differential antenna sizing (D = 3 cm).

D [cm]	α [deg]	ρ [deg]	d [mm]	W_p [mm]	d_{in} [cm]	W_{GND} [cm]	L_{GND} [cm]	L [cm]
3	45	45	1	3	1	7.1	2.3	7.9

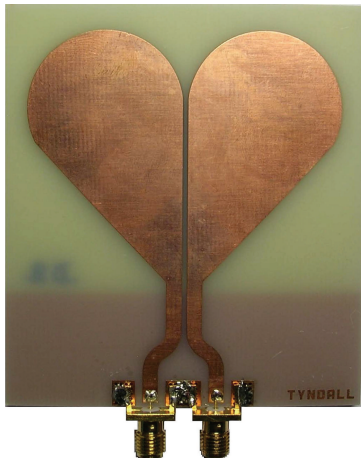

Figure 3: Photograph of the physical implementation of the folded planar differential antenna (ρ = 45°, D = 3 cm).

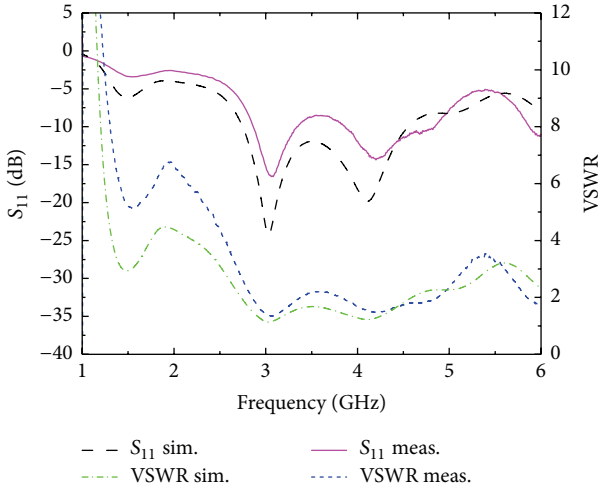

Figure 4: Measured and simulated S_{11} and VSWR versus frequency of the folded planar differential antenna (ρ = 45°, D = 3 cm).

Two microstrip feeding lines were added in order to allow the connection of the antenna to a Vector Network Analyzer (VNA) by means of 2.92 mm connectors (horizontal) and carry out the experimental tests. Width of the microstrip line feeding paths (W_p) is equal to 3 mm in order to exhibit a characteristic impedance of Z_c = 50 Ω. The distance between the two inputs of the antenna is equal to d_{in} = 1 cm to allow the placement of two adjacent connectors, as shown in Figure 1. The characteristic sizes of the UWB antenna are reported in Table 1. The simulated and measured S_{11} parameter and VSWR are reported in Figure 4. The measured S_{11} exhibits a magnitude lower than −10 dB almost in the whole band of

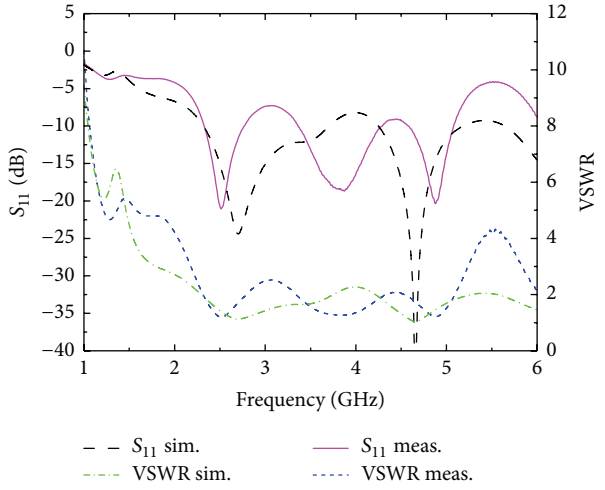

Figure 5: Measured and simulated S_{11} and VSWR as a function of frequency for the folded planar differential antenna (ρ = 45°, D = 4 cm).

interest, roughly from 3 to 5 GHz [17, 18]. Figure 4 reports also the results for the voltage wave standing ratio (VSWR), which is lower than two almost in the whole band of interest.

2.2. Folded Radiating Elements: ρ = 45° and D = 4 cm. Simulated and measured S_{11} parameter as a function of frequency of the antenna with folded radiating elements (ρ = 45° with D = 4 cm) are shown in Figure 5. All the other design parameters are unchanged with respect to the folded antenna with D = 3 cm. The measurements show S_{11} lower than approximately −7.5 dB from 2.4 to 5 GHz. In particular, S_{11} < −10 dB roughly from 2.3 to 2.7 GHz and from 3.3 to 5.1 GHz. Figure 5 reports also the measurement results for the VSWR which is lower than about 2 over the same bands reported above, for the measured antenna. As expected, the results confirm that the bandwidth, for this design variation with D = 4 cm, is extended roughly for about 0.5 GHz towards the lower frequencies with respect to the original design with D = 3 cm. This result shows that this design variation has the potential to be compatible with multiband operations for both industrial scientific medical (ISM) narrow band at 2.4 GHz [19, 20] and the lower portion of the UWB band from about 3 to 5 GHz [3].

2.3. Antipodal Radiating Elements: ρ = 180° and D = 3 cm. The physical implementation of the antipodal planar differential antenna is shown in Figure 6. The design parameters are summarized in Table 2. S_{11} parameter and VSWR resulting from simulations and measurements are shown in Figure 7. $|S_{11}|$ is lower than −10 dB in the frequency band from about 1.1 to 1.44 GHz. The antenna is thus compatible with operation

Table 2: Antipodal planar differential antenna sizing (D = 3 cm).

D [cm]	α [deg]	ρ [deg]	d_{in} [cm]	W_{GND} [cm]	L_{GND} [cm]	W [cm]	L [cm]
3	45	180	1	0.8	1.4	4	11.2

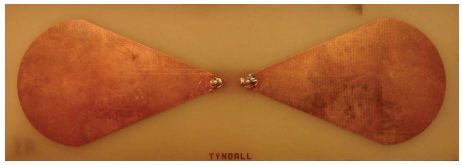

Figure 6: Antipodal planar differential antenna: photograph of the physical implementation. The two 2.92 mm connectors (vertical) are soldered on the bottom plane.

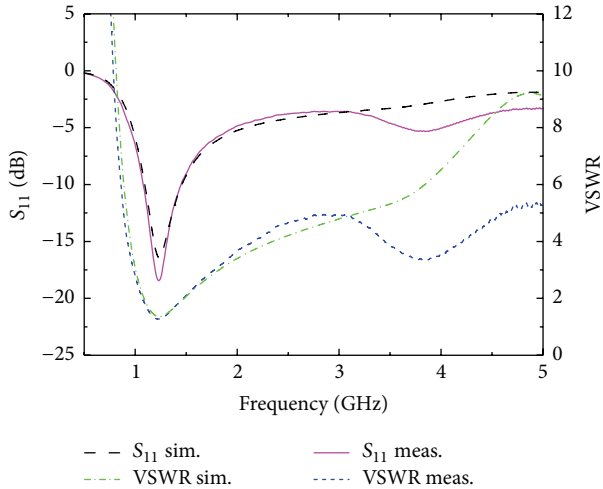

Figure 7: Measured and simulated S_{11} and VSWR as a function of frequency for the antipodal planar differential antenna (ρ = 180°, D = 3 cm).

in 1.2 GHz lower L-band adopted by satellite applications for Global Positioning and Navigation Satellite Systems (GNSS) [21].

2.4. Antipodal Radiating Elements: ρ = 180° and D = 4 cm. In this design, we have D = 4 cm, L = 14.6 cm, and W = 5 cm. All the other design parameters are unchanged with respect to those summarized for the previous case in Table 2.

S_{11} parameter and VSWR resulting from simulations and measurements are shown in Figure 8. We get $|S_{11}| < -10$ dB in the frequency band from 0.8 to 1.06 GHz.

It is worth observing how the increase of diameter (D = 4 cm), with respect to the case with D = 3 cm, enables the potential coverage of the ISM band at 868 MHz [22, 23].

The discrepancies between measured and simulated S_{11}, for the discussed antenna variations, are the results of a number of factors influencing the impedance matching of the antenna prototype during measurements, which are not taken into account in the simulation model. Namely, the presence of SMA connectors and solders in the real prototype,

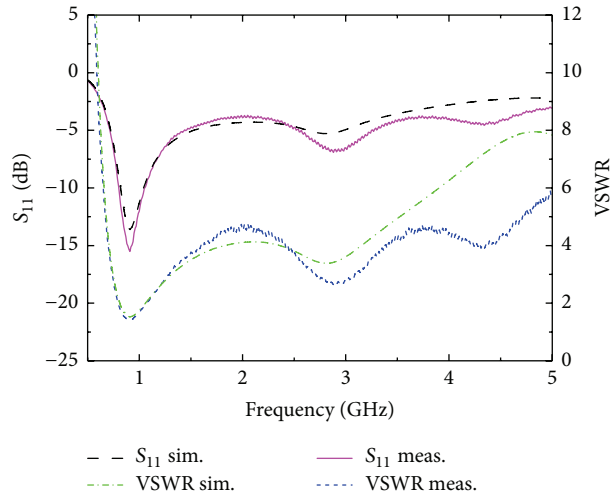

Figure 8: Measured and simulated S_{11} and VSWR as a function of frequency for the antipodal planar differential antenna (ρ = 180°, D = 4 cm).

not accounting for in the simulation, can result in deviation of input impedances, with a consequent variation in measured S-parameters with respect to the simulated ones. Measurement cables, although accurately shielded during measurements, can also be partly responsible for such deviations, it is very difficult to completely eliminate coupling between them and the radiating elements. However, the discrepancies can be still considered more than acceptable.

3. On-Body Characterization

All four variations of planar differential antennas summarized in the previous section were characterized through on-body experimental tests, in order to investigate the impact of the proximity to the human body on the antenna performance and explore their potentialities for future implementations through ad hoc designs on flexible substrates or textile fabrics [14] and exploitation in wearable applications [21].

The measurements were carried out in anechoic chamber, where the antennas under test were placed on the chest area of a real human subject, with fixed distance of 15 mm between the printed circuit board of the antenna and the body surface, achieved by means of a dielectric spacer placed between them. Each antenna was mounted on the spacer, and all together were placed on the chest of the human body. The radiating element of the antenna is on the opposite side of the interface with the spacer. z-axis is oriented away from and perpendicularly to the body surface, and y-axis is pointing upwards, as shown in Figures 9 and 10(a). The main physical and dielectric characteristics parameters of the antenna and spacer fabric are reported in Table 3.

Table 3: Physical and electric parameters of antenna and spacer.

	Dielectric layers		Conductive layers	
	Substrate	*Spacer*		
Material	FR4	"3 mesh®" spacer fabric–Müller Textil	*Material*	Copper
T [mm]	1.6	15	t [μm]	35
ε_r	4.4	≈1.05	σ [S/m]	5.96×10^7
$\tan\delta$	0.02	≈0		

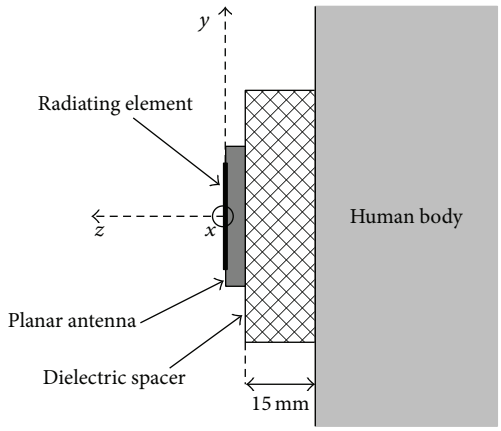

Figure 9: Cross section of planar antenna, dielectric spacer, and human body.

It is worth remarking that the purpose of the experimental on-body characterization was to test a realistic situation, that is, with the antenna placed on a real human body, where slight distance variations occur due to small body movements due to respiration and spacer compression. The scheme in Figure 9 is therefore a simple illustrative representation of the antenna placement on the body, not displaying the abovementioned realistic effects.

The reflection coefficient as a function of frequency and the differential gain pattern on azimuth plane (xz), $G_d(\theta)$ were determined for all four antennas. The gain pattern was derived by measuring, by means of an Agilent PNAX network analyzer, transmission coefficient S_{d1} between the single output of a standard-gain horn and the differential terminals of the antenna under test, for different azimuth (θ) orientations, then rescaling the measured value by calibrating path loss, gain of the transmitting horn, and mismatch factors at both ends, in order to obtain the gain pattern. For all the measurements, particular care was taken to avoid as much possible interference and scattering as possible from measurement cables which, for this purpose, were covered by radiofrequency absorbing material. In addition, ferrite chokes were placed around the measurement cables in order to furtherly reduce scattering and undesired coupling with the antenna.

3.1. Folded Radiating Elements: $\rho = 45^\circ$ and $D = 3$ cm. The measured reflection coefficient and azimuth gain pattern at $f = 3$ GHz, for the smaller antenna with folded radiating elements, on human body, are shown in Figures 11 and 12, respectively. One can see how the reflection coefficient, compared to the open-space measurements, is affected by small variations due to the proximity with human body. However, the reflection coefficient remains more than acceptable, being $S_{11} < -10$ dB in the frequency band from 2.85 to 4.53 GHz.

The measured differential gain pattern at $f = 3$ GHz (i.e., about the lowest resonance frequency), shown in Figure 12, exhibits a main lobe in the half space oriented away from the human body (i.e., $-90^\circ < \theta < +90^\circ$). The maximum gain for $\theta = 0^\circ$ is about 4.14 dBi, which is increased by an amount of about 2.7 dB with respect to the open-space case, for which the maximum gain was about 1.43 dBi. It is worth noting that, in this case, the human body is acting as a reflector, producing an increase of the maximum gain and directivity. The backscattering gain is largely attenuated by the human body which absorbs most of the power radiated by the antenna.

Thereby, this antenna is also capable of operating when worn by a human body, for UWB off-body wireless communications in the lower portion of the UWB frequency spectrum (e.g., 3–5 GHz).

3.2. Folded Radiating Elements: $\rho = 45^\circ$ and $D = 4$ cm. Figures 13 and 14 show the measured differential reflection coefficient and the azimuth gain pattern of the larger version of the antenna with folded elements (i.e., with $D = 4$ cm). Similar to the folded antenna with $D = 3$ cm, the reflection coefficient and consequently the VSWR undergo a slight variation due to the presence of the human body. In particular, we have $S_{11} < -8.3$ dB and VSWR < 2.1 in the lower portion of the UWB band from 3 to 5 GHz, which indicates more than acceptable performance of this antenna when worn on human body. Moreover, $S_{11} < -10$ dB in the bands from 2.3 to 2.7 GHz and from 3.3 to 5 GHz. Concerning the measured gain pattern of the on-body antenna shown in Figure 14, at $f = 2.5$ GHz, this has a main lobe directed away from the body with a maximum of about 1.5 dBi in broadside direction.

The maximum gain is increased of about 3.5 dB when compared to open-space measurements, indicating reflection from the human body. This antenna variation, similar to the antenna with larger folded elements, is potentially suitable for on-body operation in UWB off-body communications in the lower UWB spectrum and 2.4 GHz ISM band.

3.3. Antipodal Radiating Elements: $\rho = 180^\circ$ and $D = 3$ cm. The on-body measured reflection coefficient and gain pattern at $f = 1.2$ GHz, compared to the open-space results, for the smaller antipodal antenna are shown in Figures 15 and 16, respectively. The reflection coefficient is affected by slight variations due to the proximity to the human body. In particular, −10 dB S_{11} band becomes slightly narrower, extending in the frequency band from 1.08 to 1.37 GHz, and the resonance frequency decreases by about 10 MHz to value of $f = 1.21$ GHz.

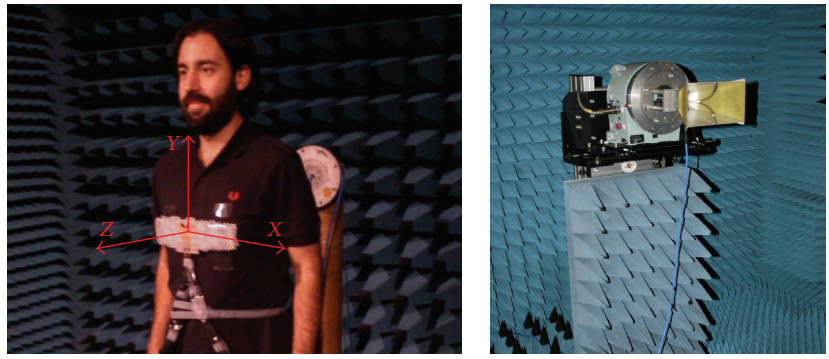

(a) (b)

Figure 10: Photographs of the experimental setup. (a) Planar differential antenna placed on a spacer and then on the chest of the human body, along with the antenna reference system. (b) Standard-gain horn antenna.

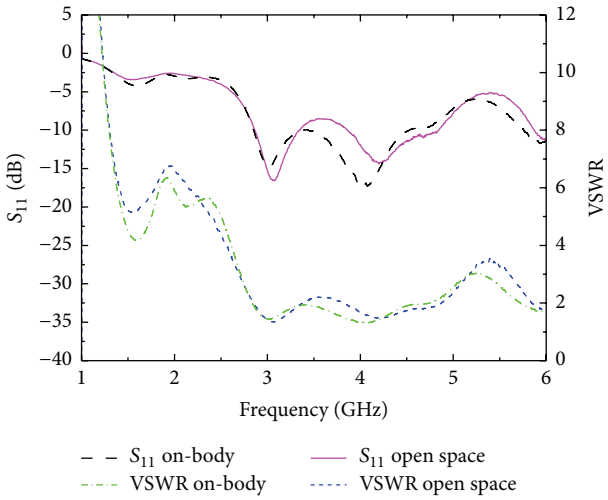

Figure 11: On-body measured S_{11} and VSWR versus frequency of the folded planar differential antenna with $\rho = 45^{\circ}$ and $D = 3$ cm.

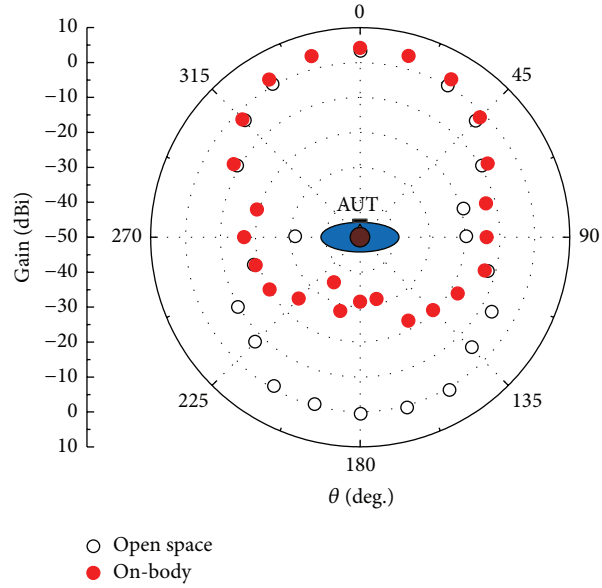

Figure 12: Measured differential gain pattern at $f = 3$ GHz in the azimuth plane (xz) for the folded planar differential antenna ($\rho = 45^{\circ}$, $D = 3$ cm).

The gain pattern, shown in Figure 16, measured at $f = 1.2$ GHz, is prone to severe attenuation of the backscattering due to the human body and has a maximum value of about 0.5 dBi, that is slightly larger than value of −0.3 dBi obtained for the open-space case. Finally, in the on-body operation, this antenna remains capable of operating reliably in 1.2 GHz lower L-band for GNSS applications.

3.4. Antipodal Radiating Elements: $\rho = 180^{\circ}$ and $D = 4$ cm. The experimental results for the bigger version of the planar differential antenna with antipodal elements ($D = 4$ cm) are shown in Figures 17 and 18.

The differential reflection coefficient, shown in Figure 17, indicates a resonance frequency of about 874 MHz, slightly decreased with respect to the open-space case, and $S_{11} < -10$ dB (or VSWR < 1.92) in the band from 820 to 954 MHz, slightly narrower than the open-space band. The proximity to the human body worsens slightly the impedance matching performance with respect to the open-space measurements. In spite of all, the body-worn antenna is still capable of providing a good coverage of the 868 MHz ISM band.

As for the gain pattern in xz plane, Figure 18 shows that the gain pattern at $f = 868$ MHz of the antenna worn on body is affected by a reduction of the maximum gain, which amounts to about −1 dBi, 2 dB lower than the value of about 1 dBi in open space. Moreover, the backscattering of the gain pattern is, similar to all other antennas, severely attenuated by the human body. This antenna variation, in on-body operation, still exhibits the characteristic performance suitable for its potential usage in the Ultra High Frequency (UHF) band at 915 MHz for Radiofrequency Identification (RFID).

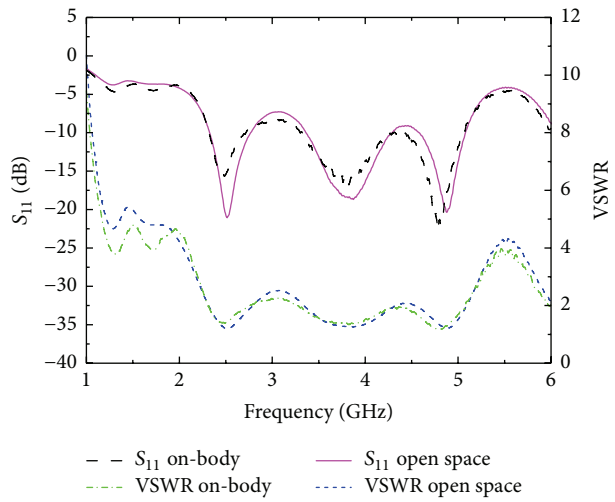

FIGURE 13: On-body measured S_{11} and VSWR versus frequency of the folded planar differential antenna with $\rho = 45^{\circ}$ and $D = 4$ cm.

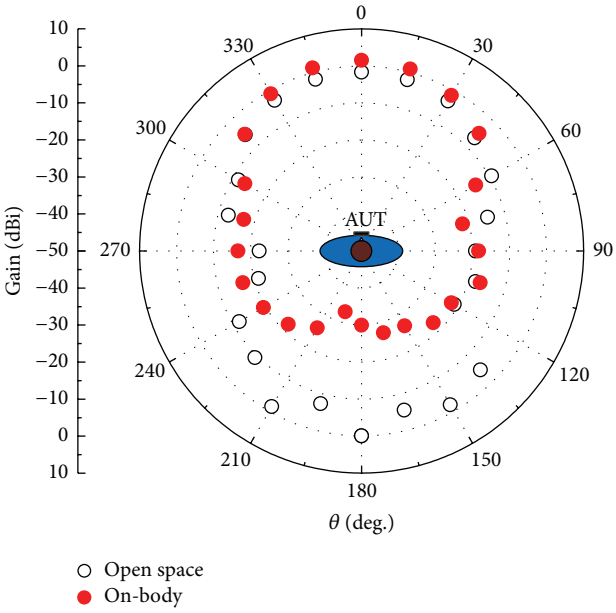

FIGURE 14: Measured differential gain pattern at $f = 2.5$ GHz in azimuth plane (xz) for the folded planar differential antenna ($\rho = 45^{\circ}$, $D = 4$ cm).

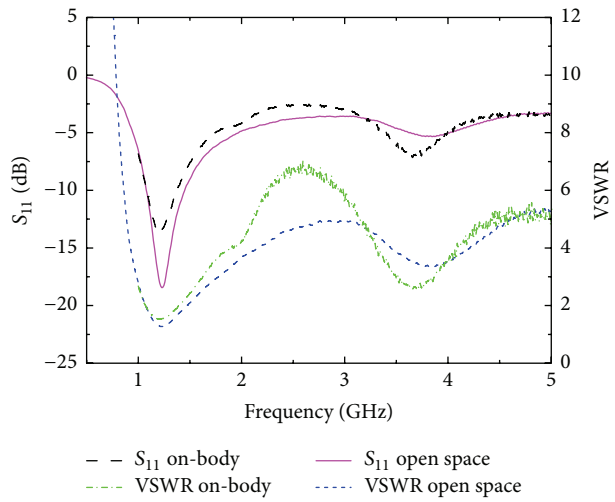

FIGURE 15: On-body measured S_{11} and VSWR versus frequency of the planar differential antenna with antipodal radiating elements ($\rho = 180^{\circ}$, $D = 3$ cm).

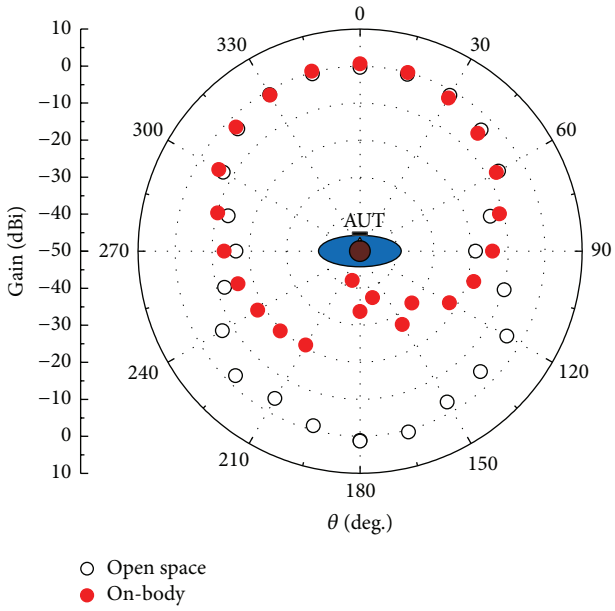

FIGURE 16: Measured differential gain pattern at $f = 1.2$ GHz in azimuth plane (xz) for the antipodal planar differential antenna ($\rho = 180^{\circ}$, $D = 3$ cm).

4. Conclusions

Four different variations of planar differential antennas, for wide and narrow band applications, differing in dimensions and orientation of the radiating elements, were experimentally characterized when worn on the chest of a human body. Measurements were performed of the differential reflection coefficient and horizontal gain pattern of the antenna, with a distance of 15 mm between antenna and human body. Results were compared with those obtained with the antenna in open space and the following observations could be made.

Concerning the impact on the performance, the presence of the human body has a clear effect on reflection coefficient and gain patterns. In particular, as for the gain pattern, the proximity to the human body produces, for all antenna variations, a severe attenuation of the backscattering portion of the gain pattern, towards the back side of the wearer, due to absorption of the radiated power by the human body. Moreover, for 3 of the 4 antennas, the maximum gain measured on-body for the lowest resonance frequency, is affected by a small increase with respect to the open-space case, indicating that the human body acts as a reflector. For the larger ($D = 4$ cm) version of the antenna with antipodal elements only, the maximum gain results in a reduction of about 2 dB with respect to the open-space measurements.

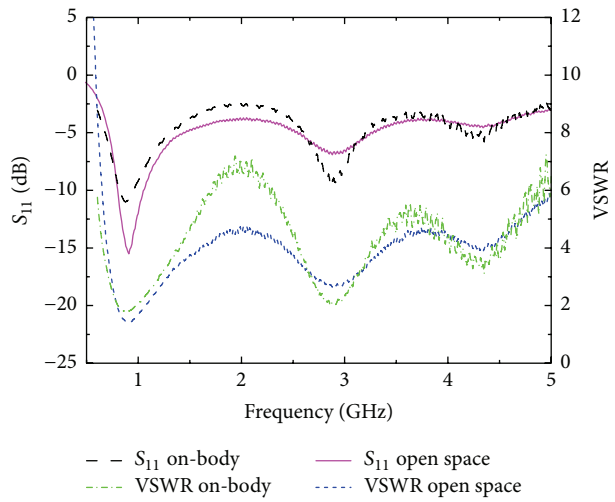

FIGURE 17: Measured and simulated S_{11} and VSWR versus frequency of the planar differential antenna with antipodal radiating elements ($\rho = 180^{\circ}$, $D = 4$ cm).

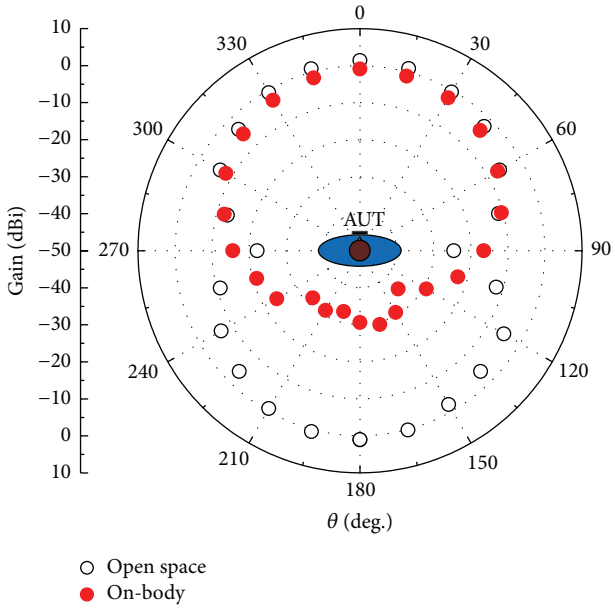

FIGURE 18: Measured differential gain pattern at $f = 0.868$ GHz in azimuth plane (xz) for the folded planar differential antenna ($\rho = 45^{\circ}$, $D = 4$ cm).

Concerning reflection coefficient, the presence of the human body results in small variations of the characteristics, with the most noticeable effect being a slight lowering of the resonance frequencies. The reflection coefficient performance remains more than acceptable for operation at the frequencies of interest.

In conclusion, the performance of all antennas remains more than acceptable when they are worn at 15 mm of distance from the chest area of a human body. This proves the potential for future wearable implementations of all considered prototypes, in particular for short range off-body communications, with applications such as monitoring of vital signs or body area network personal communications. Moreover, the four antenna variations allow the coverage of several frequency bands of interests, such as the lower portion of the UWB from 3 to 5 GHz, the 868 MHz and 2.45 GHz ISM bands, the 1.2 GHz band (lower L-band) for the Global Positioning and Navigation Satellite System (GNSS), and the UHF band at 915 MHz for Radiofrequency Identification (RFID).

Competing Interests

The authors declare that there are no competing interests regarding the publication of this paper.

Acknowledgments

The authors are grateful to Keysight Technologies and Microlease for their generous donations of hardware equipment and software computer-aided design tools in support of the research activities carried out at the Marconi Lab, Tyndall National Institute. This work was supported in part by the Science Foundation Ireland under Grant SFI07/SK/I1258, in part by the Irish Research Council (IRC) under Grant R13485, and Higher Education Authority (HEA). This publication has emanated also from research supported in part by another research grant from SFI and is cofunded under the European Regional Development Fund under Grant no. 13/RC/2077.

References

[1] P. Bernardi, R. Cicchetti, S. Pisa, E. Pittella, E. Piuzzi, and O. Testa, "Design, realization, and test of a UWB radar sensor for breath activity monitoring," *IEEE Sensors Journal*, vol. 14, no. 2, pp. 584–596, 2014.

[2] D. Zito, D. Pepe, M. Mincica et al., "SoC CMOS UWB pulse radar sensor for contactless respiratory rate monitoring," *IEEE Transactions on Biomedical Circuits and Systems*, vol. 5, no. 6, pp. 503–510, 2011.

[3] D. Zito and D. Pepe, "Planar differential antenna design and integration with pulse radar microchip sensor," *IEEE Sensors Journal*, vol. 14, no. 8, pp. 2477–2487, 2014.

[4] D. Zito and D. Pepe, "Monitoring respiratory pattern in adult and infant via contactless detection of thorax and abdomen movements through SoC UWB pulse radar sensor," in *Proceedings of the IEEE Topical Conference on Biomedical Wireless Technologies, Networks, and Sensing Systems (BioWireleSS '14), IEEE Radio Wireless Week (RWW '14)*, pp. 1–3, Newport Beach, Calif, USA, January 2014.

[5] G. Cappelletti, D. Caratelli, R. Cicchetti, and M. Simeoni, "A low-profile printed drop-shaped dipole antenna for wide-band wireless applications," *IEEE Transactions on Antennas and Propagation*, vol. 59, no. 10, pp. 3526–3535, 2011.

[6] D. Zito and D. Pepe, "UWB pulse radio transceivers and antennas: considerations on design and implementation," in *Proceedings of the 8th European Conference on Antennas and Propagation (EuCAP '14)*, pp. 1633–1637, The Hague, The Netherlands, April 2014.

[7] D. Pepe, L. Vallozzi, H. Rogier, and D. Zito, "Planar differential antenna for short-range UWB pulse radar sensor," *IEEE Antennas and Wireless Propagation Letters*, vol. 12, pp. 1527–1530, 2013.

[8] D. Pepe, L. Vallozzi, H. Rogier, and D. Zito, "Design variations on planar differential antenna with potential for multiple, wide, and narrow band coverage," *International Journal of Antennas and Propagation*, vol. 2015, Article ID 478453, 13 pages, 2015.

[9] L. Vallozzi, H. Rogier, and C. Hertleer, "Dual polarized textile patch antenna for integration into protective garments," *IEEE Antennas and Wireless Propagation Letters*, vol. 7, pp. 440–443, 2008.

[10] T. Kellomäki, "On-body performance of a wearable single-layer RFID tag," *IEEE Antennas and Wireless Propagation Letters*, vol. 11, pp. 73–76, 2012.

[11] X. Li, L. Zwirello, M. Jalilvand, and T. Zwick, "Design and near-field characterization of a planar on-body UWB slot-antenna for stroke detection," in *Proceedings of the IEEE International Workshop on Antenna Technology (iWAT '12)*, pp. 201–204, Tucson, Ariz, USA, March 2012.

[12] H. Liu, X. Y. Liu, and Y. Fan, "A miniaturized differentially fed dual-band fractal antenna for in-body communications," in *Proceedings of the 2015 IEEE MTT-S International Microwave Workshop Series on Advanced Materials and Processes for RF and THz Applications (IMWS-AMP)*, Microwave Workshop Series, pp. 1–3, Suzhou, China, July 2015.

[13] A. Iftikhar, M. M. Masud, M. N. Rafiq, S. Asif, B. D. Braaten, and M. S. Khan, "Radiation performance and Specific Absorption Rate (SAR) analysis of a compact dual band balanced antenna," in *Proceedings of the IEEE International Conference on Electro/Information Technology (EIT '15)*, pp. 672–675, Dekalb, Ill, USA, May 2015.

[14] J. Lanza, L. Sánchez, L. Muñoz et al., "Large-scale mobile sensing enabled internet-of-things testbed for smart city services," *International Journal of Distributed Sensor Networks*, vol. 2015, Article ID 785061, 15 pages, 2015.

[15] A. Zanella, N. Bui, A. Castellani, L. Vangelista, and M. Zorzi, "Internet of things for smart cities," *IEEE Internet of Things Journal*, vol. 1, no. 1, pp. 22–32, 2014.

[16] C. Feránndez-Prades, H. Rogier, A. Collado, and M. M. Tentzeris, "Flexible substrate antennas," *International Journal of Antennas and Propagation*, vol. 2012, Article ID 746360, 2 pages, 2012.

[17] F. Zito, D. Pepe, and D. Zito, "UWB CMOS monocycle pulse generator," *IEEE Transactions on Circuits and Systems. I. Regular Papers*, vol. 57, no. 10, pp. 2654–2664, 2010.

[18] D. Pepe and D. Zito, "22.7-db gain-19.7-dbm ICP_{1dB} UWB CMOS LNA," *IEEE Transactions on Circuits and Systems II: Express Briefs*, vol. 56, no. 9, pp. 689–693, 2009.

[19] X. L. Quan, R. L. Li, Y. H. Cui, and M. M. Tentzeris, "Analysis and design of a compact dual-band directional antenna," *IEEE Antennas and Wireless Propagation Letters*, vol. 11, pp. 547–550, 2012.

[20] C.-K. Wu, T.-F. Chien, C.-L. Yang, and C.-H. Luo, "Design of novel S-shaped quad-band antenna for MedRadio/WMTS/ISM implantable biotelemetry applications," *International Journal of Antennas and Propagation*, vol. 2012, Article ID 564092, 12 pages, 2012.

[21] A. Dierck, A. H. Rogier, and F. A. Declercq, "A wearable active antenna for global positioning system and satellite phone," *IEEE Transactions on Antennas and Propagation*, vol. 61, no. 2, pp. 532–538, 2013.

[22] T. Kaufmann, D. C. Ranasinghe, M. Zhou, and C. Fumeaux, "Wearable quarter-wave folded microstrip antenna for passive UHF RFID applications," *International Journal of Antennas and Propagation*, vol. 2013, Article ID 129839, 11 pages, 2013.

[23] F. Alimenti, M. Virili, G. Orecchini et al., "A new contactless assembly method for paper substrate antennas and UHF RFID chips," *IEEE Transactions on Microwave Theory and Techniques*, vol. 59, no. 3, pp. 627–637, 2011.